
QCS-SGM+: Improved Quantized Compressed Sensing with Score-Based Generative Models

Xiangming Meng

The Zhejiang University-University of Illinois Urbana-Champaign Institute (ZJUI)
Zhejiang University, China
xiangmingmeng@intl.zju.edu.cn

Yoshiyuki Kabashima

Institute for Physics of Intelligence and Department of Physics
The University of Tokyo, Japan
kaba@phys.s.u-tokyo.ac.jp

Abstract

In practical compressed sensing (CS), the obtained measurements typically necessitate quantization to a limited number of bits prior to transmission or storage. This nonlinear quantization process poses significant recovery challenges, particularly with extreme coarse quantization such as 1-bit. Recently, an efficient algorithm called QCS-SGM was proposed for quantized CS (QCS) which utilizes score-based generative models (SGM) as an implicit prior. Due to the adeptness of SGM in capturing the intricate structures of natural signals, QCS-SGM substantially outperforms previous QCS methods. However, QCS-SGM is constrained to (approximately) row-orthogonal sensing matrices as the computation of the likelihood score becomes intractable otherwise. To address this limitation, we introduce an advanced variant of QCS-SGM, termed QCS-SGM+, capable of handling general matrices effectively. The key idea is a Bayesian inference perspective on the likelihood score computation, wherein an expectation propagation algorithm is employed for its approximate computation. We conduct extensive experiments on various settings, demonstrating the substantial superiority of QCS-SGM+ over QCS-SGM for general sensing matrices beyond mere row-orthogonality. *The code is available at <https://github.com/mengxiangming/QCS-SGM-plus>.*

1 Introduction

Compressed sensing (CS) has emerged as an ubiquitous paradigm in signal processing and machine learning, aiming to accurately reconstruct high-dimensional signals from a limited number of measurements Donoho (2006); Candès & Wakin (2008). The success of CS hinges on the assumption that, while the target signal may be high-dimensional, it possesses an inherent low-dimensional representation such as sparsity or low-rankness. Conventional CS models typically assume direct access to analog (continuous) measurements with infinite precision. In practice, however, analog measurements must be quantized into a finite number of digital bits using an analog-to-digital converter (ADC or quantizer) before further transmission, storage, or processing can occur (Boufounos & Baraniuk, 2008; Zymnis et al., 2009; Dai & Milenkovic, 2011). In the extreme case, measurements are quantized into a single bit, retaining only the sign information while disregarding the magnitude Boufounos & Baraniuk (2008). Interestingly, 1-bit CS have gained attention due to their simplicity in hardware implementation and robustness against multiplicative errors Boufounos & Baraniuk (2008); Zymnis et al. (2009). Nevertheless, such nonlinear quantization operation invariably leads to information loss, thereby undermining the effectiveness of standard CS algorithms designed for

analog measurements. To address this issue, a plethora of quantized CS (QCS) algorithms have been developed by explicitly considering the quantization effect (Boufounos & Baraniuk, 2008; Zymnis et al., 2009; Dai & Milenkovic, 2011; Plan & Vershynin, 2012, 2013; Jacques et al., 2013; Xu & Kabashima, 2013; Xu et al., 2014; Awasthi et al., 2016; Meng et al., 2018; Jung et al., 2021; Liu et al., 2020; Liu & Liu, 2022; Zhu et al., 2022; Meng & Kabashima, 2023). Among these, the recently proposed algorithm QCS-SGM Meng & Kabashima (2023) demonstrates exceptional state-of-the-art (SOTA) reconstruction performance under low-precision quantization levels. The key idea of QCS-SGM lies in utilizing the powerful score-based generative models (SGM, also known as diffusion models) (Song & Ermon, 2019, 2020; Sohl-Dickstein et al., 2015; Ho et al., 2020; Nichol & Dhariwal, 2021) as an implicit prior for the target signal. Intuitively, from a Bayesian perspective, the more accurate the prior obtained, the fewer observations required. Owing to SGM’s ability to capture the intricate structure of the target signal \mathbf{x} beyond simple sparsity, QCS-SGM can accurately reconstruct \mathbf{x} even from a small number of severely quantized noisy measurements.

While QCS-SGM exhibits remarkable performance, it has a notable limitation: it is derived under the assumption that the sensing matrix \mathbf{A} is (approximately) row-orthogonal, such as Fourier or i.i.d. zero-mean Gaussian matrices. However, for more general matrices, QCS-SGM’s performance may deteriorate, as its computation of the *likelihood score* (defined later in (4)) becomes less accurate (Meng & Kabashima, 2023). Although row-orthogonal matrices are prevalent in CS, there are situations where one might encounter other types of matrices due to non-ideal physical constraints or design choices. Indeed, the investigation of general sensing matrices has been an active and important topic in CS, such as the popular ill-conditioned right-rotational invariant (RRI) matrices and correlated matrices, among others (Manoel et al., 2015; Schniter et al., 2016; Tanaka, 2018; Ihara et al., 2018; Rangan et al., 2019; Venkataraman et al., 2022; Zhu et al., 2022; Fan, 2022). Despite these advances, much of the existing work concentrates on standard CS or QCS with handcrafted sparsity. The study of QCS using SGM (diffusion models) for general sensing matrices, however, still remains a largely untouched research area.

1.1 Contributions

Our main contributions are summarized as follows.

- We propose an advanced variant of QCS-SGM, designated as QCS-SGM+, which addresses the inherent limitation of the original QCS-SGM. Specifically, by treating the likelihood score computation as a Bayesian inference problem, QCS-SGM+ utilizes the well-established expectation propagation (EP) algorithm (Minka, 2001) to yield a more refined approximation of the otherwise intractable likelihood score for general matrices.
- We validate the effectiveness of the proposed QCS-SGM+ in various experimental settings, encompassing diverse real-world datasets, distinct general matrices, and different noise levels. In each scenario, QCS-SGM+ consistently demonstrates remarkably superior performance over existing methods. The code is open-sourced at <https://github.com/mengxiangming/QCS-SGM-plus>.

1.2 Related works

Quantized compressed sensing (QCS) was first introduced in Boufounos & Baraniuk (2008); Zymnis et al. (2009), after which it has become an important research topic and various QCS algorithms have been proposed, including some theoretical analysis (Dai & Milenkovic, 2011; Plan & Vershynin, 2012, 2013; Jacques et al., 2013; Xu & Kabashima, 2013; Xu et al., 2014; Awasthi et al., 2016; Meng et al., 2018; Jung et al., 2021; Liu et al., 2020; Liu & Liu, 2022; Zhu et al., 2022). With the recent advent of deep generative models (Goodfellow et al., 2014; Kingma & Welling, 2013; Rezende & Mohamed, 2015; Song & Ermon, 2019, 2020; Sohl-Dickstein et al., 2015; Ho et al., 2020; Nichol & Dhariwal, 2021), there has been a rising interest in CS methods with data-driven priors (Bora et al., 2017; Hand & Joshi, 2019; Asim et al., 2020; Pan et al., 2021; Meng & Kabashima, 2022). Specifically, following the pioneering CSGM framework (Bora et al., 2017), the prior $p(\mathbf{x})$ of \mathbf{x} is learned through a generative model, such as VAE (Kingma & Welling, 2013), GAN (Goodfellow et al., 2014), and score-based generative models (SGM) or diffusion models (DM) (Song & Ermon, 2019, 2020; Sohl-Dickstein et al., 2015; Ho et al., 2020; Nichol & Dhariwal, 2021). In the case of QCS, Liu et al. (2020); Liu & Liu (2022) extended the CSGM framework to non-linear observations such as 1-bit CS using VAE and GAN (in particular DCGAN (Radford et al., 2015)). Surprisingly, SGM or DM

(Song & Ermon, 2019, 2020; Ho et al., 2020; Nichol & Dhariwal, 2021) have demonstrated superior effectiveness, even surpassing state-of-the-art GAN (Goodfellow et al., 2014) and VAE (Kingma & Welling, 2013) in generating diverse natural sources. In line with this, Meng & Kabashima (2023) recently proposed a novel algorithm, QCS-SGM, employing SGM as an implicit prior, achieving state-of-the-art reconstruction performances for QCS. However, its application remains confined to (approximate) row-orthogonal sensing matrices.

2 Background and Problem Setup

2.1 System model

The problem of quantized CS (QCS) can be mathematically formulated as follows (Boufounos & Baraniuk, 2008; Zymnis et al., 2009)

$$\mathbf{y} = \mathbf{Q}(\mathbf{A}\mathbf{x} + \mathbf{n}), \quad (1)$$

where the goal is to recover an unknown high-dimensional signal $\mathbf{x} \in \mathbb{R}^{N \times 1}$ from a set of quantized measurements $\mathbf{y} \in \mathbb{R}^{M \times 1}$, where $\mathbf{A} \in \mathbb{R}^{M \times N}$ is a known linear sensing matrix, $\mathbf{n} \sim \mathcal{N}(\mathbf{n}; 0, \sigma^2 \mathbf{I})$ is an i.i.d. additive Gaussian noise, and $\mathbf{Q}(\cdot) : \mathbb{R}^{M \times 1} \rightarrow \mathcal{Q}^{M \times 1}$ is an *element-wise* quantizer function which maps each element into a finite (or countable) set of codewords \mathcal{Q} , i.e., $y_m = \mathbf{Q}(z_m + n_m) \in \mathcal{Q}$, or equivalently $(z_m + n_m) \in \mathbf{Q}^{-1}(y_m)$, $m = 1, 2, \dots, M$, where z_m is the m -th element of $\mathbf{z} = \mathbf{A}\mathbf{x}$. Same as Meng & Kabashima (2023), we consider the uniform quantizer with Q quantization bits (resolution). The quantization codewords $\mathcal{Q} = \{q_r\}_{r=1}^{2^Q}$ consist of 2^Q elements, each with a quantization interval $\mathbf{Q}^{-1}(q_r) = [l_{q_r}, u_{q_r}]$, where l_{q_r} and u_{q_r} are the lower and upper quantization threshold associated with the codeword q_r . In the extreme 1-bit case when $Q = 1$, only the sign values are observed so that (1) reduces to

$$\mathbf{y} = \text{sign}(\mathbf{A}\mathbf{x} + \mathbf{n}), \quad (2)$$

which corresponds to the well-known 1-bit CS and the quantization codewords are $\mathcal{Q} = \{-1, +1\}$.

2.2 QCS-SGM: Quantized CS with SGM

Compared to standard CS without quantization, QCS is particularly more challenging due to two key factors: (1) quantization leads to information loss, especially with low quantization resolution; (2) the nonlinearity of quantization operations can cause standard CS algorithms to deteriorate when applied directly. Recently, inspired by the prowess of SCM (Song & Ermon, 2019; Song et al., 2020) in density estimation, Meng & Kabashima (2023) proposed an efficient method called QCS-SGM for QCS which can accurately reconstruct the target signal from a small number of severely quantized noisy measurements. The basic idea of QCS-SGM is to perform posterior sampling from $p(\mathbf{x} \mid \mathbf{y})$ by using a learned SGM as an implicit prior (Meng & Kabashima, 2023). Specifically, by utilizing the annealed Langevin dynamics (ALD) (Song et al., 2020), the posterior samples can be iteratively obtained as follows

$$\mathbf{x}_t = \mathbf{x}_{t-1} + \alpha_t \nabla_{\mathbf{x}_{t-1}} \log p(\mathbf{x}_{t-1} \mid \mathbf{y}) + \sqrt{2\alpha_t} \mathbf{z}_t, \quad 1 \leq t \leq T, \quad (3)$$

where the conditional (*posterior*) score $\nabla_{\mathbf{x}_t} \log p(\mathbf{x}_t \mid \mathbf{y})$ is required. Using the Bayesian rule, the $\nabla_{\mathbf{x}_t} \log p(\mathbf{x}_t \mid \mathbf{y})$ is decomposed into two terms

$$\underbrace{\nabla_{\mathbf{x}_t} \log p(\mathbf{x}_t \mid \mathbf{y})}_{\text{posterior score}} = \underbrace{\nabla_{\mathbf{x}_t} \log p(\mathbf{x}_t)}_{\text{prior score}} + \underbrace{\nabla_{\mathbf{x}_t} \log p(\mathbf{y} \mid \mathbf{x}_t)}_{\text{likelihood score}}, \quad (4)$$

which include the unconditional score $\nabla_{\mathbf{x}_t} \log p(\mathbf{x}_t)$ (termed as *prior score* in Meng & Kabashima (2023)), and the conditional score $\nabla_{\mathbf{x}_t} \log p(\mathbf{y} \mid \mathbf{x}_t)$ (termed as *likelihood score* in Meng & Kabashima (2023)), respectively. While the prior score $\nabla_{\mathbf{x}_t} \log p(\mathbf{x}_t)$ can be readily computed using a pre-trained score network such as NCSN (Song & Ermon, 2019) or NCSNv2 (Song et al., 2020), the likelihood score $\nabla_{\mathbf{x}_t} \log p(\mathbf{y} \mid \mathbf{x}_t)$ is generally intractable. To circumvent this difficulty, Meng & Kabashima (2023) proposed a simple yet effective approximation of $\nabla_{\mathbf{x}_t} \log p(\mathbf{y} \mid \mathbf{x}_t)$ under an uninformative prior assumption, whereby \mathbf{x}_t is approximated as $\mathbf{x}_t = \mathbf{x} + \beta_t \tilde{\mathbf{n}}$, where $\tilde{\mathbf{n}} \sim \mathcal{N}(\mathbf{0}, \mathbf{I})$. As a result, substituting it into (1), we obtain an equivalent representation as

$$\mathbf{y} = \mathbf{Q}(\mathbf{A}\mathbf{x}_t + \tilde{\mathbf{n}}_t), \quad (5)$$

where $\tilde{\mathbf{n}}_t \sim \mathcal{N}(\mathbf{0}, \sigma^2 \mathbf{I} + \beta_t^2 \mathbf{A} \mathbf{A}^T)$ and $\{\beta_t\}_{t=1}^T$ are a sequence of noise scales satisfying $\beta_{\max} = \beta_1 > \beta_2 > \dots > \beta_T = \beta_{\min} > 0$ (Song et al., 2020). From (5), an approximation $\tilde{p}(\mathbf{y}|\mathbf{z}_t = \mathbf{A}\mathbf{x}_t)$ (called *pseudo-likelihood*) of $p(\mathbf{y}|\mathbf{x}_t)$ can be obtained as (Meng & Kabashima, 2023)

$$p(\mathbf{y}|\mathbf{x}_t) \simeq \tilde{p}(\mathbf{y}|\mathbf{z}_t = \mathbf{A}\mathbf{x}_t) = \int \prod_{m=1}^M \mathbb{1}((z_{t,m} + \tilde{n}_{t,m}) \in Q^{-1}(y_m)) \mathcal{N}(\tilde{\mathbf{n}}_t; \mathbf{0}, \mathbf{C}_t^{-1}) d\tilde{\mathbf{n}}_t, \quad (6)$$

where $\mathbf{C}_t^{-1} = \sigma^2 \mathbf{I} + \beta_t^2 \mathbf{A} \mathbf{A}^T$ and $z_{t,m}, \tilde{n}_{t,m}$ as the m -th elements of $\mathbf{z}_t, \tilde{\mathbf{n}}_t$, respectively, and $\mathbb{1}(\cdot)$ denotes the indicator function, i.e., it equals 1 if the event in the argument is true and equals 0 otherwise. Furthermore, under the assumption that \mathbf{A} is a row-orthogonal matrix such that $\mathbf{A} \mathbf{A}^T$ (and thus the covariance matrix \mathbf{C}_t^{-1}) becomes diagonal, Meng & Kabashima (2023) obtained a closed-form solution of the *pseudo-likelihood score* $\nabla_{\mathbf{x}_t} \log \tilde{p}(\mathbf{y}|\mathbf{z}_t = \mathbf{A}\mathbf{x}_t)$, which leads to QCS-SGM. Unfortunately, there is no closed-form solution for general matrices \mathbf{A} , which is the fundamental limitation of QCS-SGM. For more details of QCS-SGM and SGM, please refer to Meng & Kabashima (2023) and Song & Ermon (2019); Song et al. (2020), respectively.

3 QCS-SGM+: Improved QCS-SGM

In this section, to dress the inherent limitation of QCS-SGM (Meng & Kabashima, 2023), we propose an enhanced variant, termed as QCS-SGM+, for general sensing matrices \mathbf{A} beyond mere row-orthogonality.

3.1 A New Perspective

Our key insight is that the pseudo-likelihood term $\tilde{p}(\mathbf{y}|\mathbf{z}_t = \mathbf{A}\mathbf{x}_t)$ (6) can be interpreted as the partition function (normalization term) of a posterior distribution concerning the random variables $\tilde{\mathbf{n}}_t$. Here, $\mathcal{N}(\tilde{\mathbf{n}}_t; \mathbf{0}, \mathbf{C}_t^{-1})$ acts as the prior distribution, and $\prod_{m=1}^M \mathbb{1}((z_{t,m} + \tilde{n}_{t,m}) \in Q^{-1}(y_m))$ serves as the factorized likelihood distribution. The corresponding factor graph is depicted in Figure 1 (a). Interestingly, for row-orthogonal matrices \mathbf{A} , the covariance matrix $\mathbf{C}_t^{-1} = \sigma^2 \mathbf{I} + \beta_t^2 \mathbf{A} \mathbf{A}^T$ becomes diagonal and thus the prior node $f_b(\tilde{\mathbf{n}}_t)$ in Figure 1 (a) also fully factorizes, i.e., the random variables $\tilde{\mathbf{n}}_t$ become independent to each other so that the high-dimensional integration in (6) reduces to a parallel computation of simple closed-form scalar integrations, which is the case of QCS-SGM (Meng & Kabashima, 2023).

However, for general matrices \mathbf{A} , since the random variables $\tilde{\mathbf{n}}_t$ are coupled together in the prior node $f_b(\tilde{\mathbf{n}}_t)$, the partition function (6) involves an intractable high-dimensional integration. In Bayesian inference, computing the partition function is a fundamental challenge and numerous approximate Bayesian methods have been proposed (Wainwright & Jordan, 2008). As a result, the new perspective on pseudo-likelihood as partition function provides us with a solution using approximate inference. That is, while an exact closed-form solution is unattainable for a general (non-diagonal) covariance matrix \mathbf{C}_t^{-1} , we can instead obtain an estimate of it using efficient approximate inference methods.

3.2 Pseudo-likelihood score via EP

Due to its efficacy and low-complexity implementation, we resort to the well-established expectation propagation (EP) (Minka, 2001) (also known as moment matching (Opper et al., 2005)) to approximately compute the partition function or pseudo-likelihood $\tilde{p}(\mathbf{y}|\mathbf{z}_t = \mathbf{A}\mathbf{x}_t)$ (6). The underlying idea is illustrated in Figure 1, where we apply EP to derive an effective factorized approximation of $\mathcal{N}(\tilde{\mathbf{n}}_t; \mathbf{0}, \mathbf{C}_t^{-1})$. As shown in Figure 1 (b), after EP, the original coupled prior node $f_b(\tilde{\mathbf{n}}_t)$ in Figure 1 (a) is decoupled into a series of fully-factorized prior nodes $f_c(\tilde{n}_{t,m})$, $m = 1 \dots M$. Consequently, a closed-form solution for the pseudo-likelihood $\tilde{p}(\mathbf{y}|\mathbf{z}_t = \mathbf{A}\mathbf{x}_t)$ (6) can be obtained, thereby enabling us to compute the pseudo-likelihood score $\nabla_{\mathbf{x}_t} \log \tilde{p}(\mathbf{y}|\mathbf{z}_t = \mathbf{A}\mathbf{x}_t)$.

It is worth pointing out that the original QCS-SGM (Meng & Kabashima, 2023) can also be viewed as decoupling the prior node $f_b(\tilde{\mathbf{n}}_t)$ in Figure 1 (a) into fully factorized nodes, but in a naive manner: it approximates \mathbf{C}_t^{-1} as a diagonal matrix based solely on its main diagonal elements. That is why the performance of QCS-SGM is contingent upon the assumption that \mathbf{C}_t^{-1} is approximately diagonal, or equivalently, \mathbf{A} is approximately row-orthogonal. The crude diagonalization in QCS-SGM completely

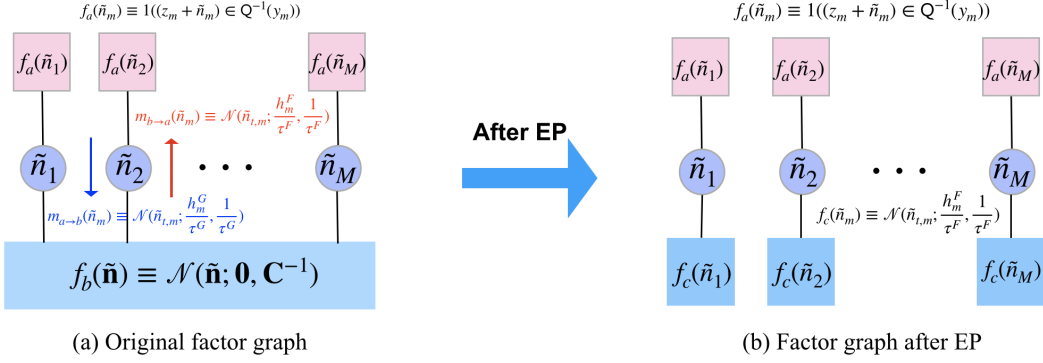


Figure 1: A schematic of the basic idea of QCS-SGM+ in computing the intractable pseudo-likelihood $\tilde{p}(\mathbf{y}|\mathbf{z}_t = \mathbf{Ax}_t)$ for general matrices. The subscript t is dropped for simplicity. We resort to EP to obtain an effective factorized approximation of $f_b(\tilde{\mathbf{n}})$ so that a closed-form solution of $\tilde{p}(\mathbf{y}|\mathbf{z}_t = \mathbf{Ax}_t)$ can be achieved, which enables the otherwise computation of intractable pseudo-likelihood score.

ignores the potential correlation among different random variables in $\tilde{\mathbf{n}}_t$. By contrast, as illustrated in the following, EP explicitly takes the potential correlation among $\tilde{\mathbf{n}}_t$ into account (Minka, 2001; Opper et al., 2005), thereby leading to better performances for general matrices \mathbf{A} .

Specifically, the details of EP are illustrated as follows. Essentially, it approximates the integral in $\tilde{p}(\mathbf{y}|\mathbf{z}_t = \mathbf{Ax}_t)$ (6) in three different ways as follows¹:

$$\tilde{p}(\mathbf{y}|\mathbf{z}_t = \mathbf{Ax}_t) \approx \begin{cases} \int \prod_{m=1}^M \mathbb{1}((z_{t,m} + \tilde{n}_{t,m}) \in Q^{-1}(y_m)) \mathcal{N}(\tilde{n}_{t,m}; \frac{h_m^F}{\tau^F}, \frac{1}{\tau^F}) d\tilde{\mathbf{n}}_t & (a) \\ \int \prod_{m=1}^M \mathcal{N}(\tilde{n}_{t,m}; \frac{h_m^G}{\tau^G}, \frac{1}{\tau^G}) \mathcal{N}(\tilde{\mathbf{n}}_t; \mathbf{0}, \mathbf{C}_t^{-1}) d\tilde{\mathbf{n}}_t & (b) \\ \int \prod_{m=1}^M \mathcal{N}(\tilde{n}_{t,m}; \frac{h_m^G}{\tau^G}, \frac{1}{\tau^G}) \mathcal{N}(\tilde{n}_{t,m}; \frac{h_m^F}{\tau^F}, \frac{1}{\tau^F}) d\tilde{\mathbf{n}}_t & (c) \end{cases} \quad (7)$$

Intuitively, (7-a) approximates the correlated multivariate Gaussian $\mathcal{N}(\tilde{\mathbf{n}}_t; \mathbf{0}, \mathbf{C}_t^{-1})$ with a product of independent Gaussians $\prod_{m=1}^M \mathcal{N}(\tilde{n}_{t,m}; \frac{h_m^F}{\tau^F}, \frac{1}{\tau^F})$, (7-b) approximates the non-Gaussian likelihood $\mathbb{1}((z_{t,m} + \tilde{n}_{t,m}) \in Q^{-1}(y_m))$ with a Gaussian likelihood $\mathcal{N}(\tilde{n}_{t,m}; \frac{h_m^G}{\tau^G}, \frac{1}{\tau^G})$, and (7-c) combines the two approximations together. In the language of factor graph and message passing (Wainwright & Jordan, 2008), as shown in Figure 1, $\mathcal{N}(\tilde{n}_{t,m}; \frac{h_m^F}{\tau^F}, \frac{1}{\tau^F})$ corresponds to the message $m_{b \rightarrow a}(\tilde{n}_m)$ from factor node f_b to factor node f_a , while $\mathcal{N}(\tilde{n}_{t,m}; \frac{h_m^G}{\tau^G}, \frac{1}{\tau^G})$ corresponds to the message $m_{a \rightarrow b}(\tilde{n}_m)$ from factor node f_a to factor node f_b . The three approximations (7-a), (7-b), and (7-c) correspond to the combined results of incoming messages in EP at factor node f_a , variable node \tilde{n}_m , factor node f_b , respectively. The key point is that, after EP, an alternative fully factorized representation is obtained as shown in Figure 1 (b), leading to a closed-form approximation of the pseudo-likelihood $\tilde{p}(\mathbf{y}|\mathbf{z}_t = \mathbf{Ax}_t)$ as follows

$$\tilde{p}(\mathbf{y}|\mathbf{z}_t = \mathbf{Ax}_t) \approx \frac{e^{\frac{(h_m^F)^2}{2\tau^F}}}{2} \left[\text{erfc}\left(\frac{-\tilde{u}_{y_m}}{\sqrt{2}}\right) - \text{erfc}\left(\frac{-\tilde{l}_{y_m}}{\sqrt{2}}\right) \right], \quad (8)$$

where

$$\tilde{u}_{y_m} = -\sqrt{\tau^F} z_{t,m} - \frac{h_m^F}{\sqrt{\tau^F}} + u_{y_m} \sqrt{\tau^F}, \quad (9)$$

$$\tilde{l}_{y_m} = -\sqrt{\tau^F} z_{t,m} - \frac{h_m^F}{\sqrt{\tau^F}} + l_{y_m} \sqrt{\tau^F}. \quad (10)$$

Therefore, from (6) and (8), the pseudo-likelihood score $\nabla_{\mathbf{x}_t} \log p_{\beta_t}(\mathbf{y} \mid \mathbf{x}_t)$ under quantized measurements \mathbf{y} in (1) can be approximated as

$$\nabla_{\mathbf{x}_t} \log p_{\beta_t}(\mathbf{y} \mid \mathbf{x}_t) \simeq \mathbf{A}^T \mathbf{G}(\beta_t, \mathbf{y}, \mathbf{A}, \mathbf{z}_t, \mathbf{h}^F, \tau^F), \quad (11)$$

¹The results might differ in a constant scaling factor which is safely ignored as it does not affect the final concerned score function.

where $\mathbf{G}(\beta_t, \mathbf{y}, \mathbf{A}, \mathbf{z}_t, \mathbf{h}^F, \tau^F) = [g_1, g_2, \dots, g_M]^T \in \mathbb{R}^{M \times 1}$ with the m -th element being

$$g_m = -\frac{\sqrt{2\tau^F} \left[\exp\left(-\frac{\tilde{u}_{y_m}^2}{2}\right) - \exp\left(-\frac{\tilde{l}_{y_m}^2}{2}\right) \right]}{\sqrt{\pi} \left[\operatorname{erfc}\left(-\frac{\tilde{u}_{y_m}}{\sqrt{2}}\right) - \operatorname{erfc}\left(-\frac{\tilde{l}_{y_m}}{\sqrt{2}}\right) \right]}. \quad (12)$$

As a result, the remaining task is to determine the associated parameters $(\mathbf{h}^F, \tau^F, \mathbf{h}^G, \tau^G)$ in (7) which can be done using EP (Minka, 2001; Opper et al., 2005) by imposing a consistency of the associated posterior mean $\mathbb{E}[\tilde{n}_{t,m}]$ and variance $\mathbb{V}[\tilde{n}_{t,m}]$ of $\tilde{n}_{t,m}$ from all the three approximations in (7), denoted as (m_m^a, χ^a) , (m_m^b, χ^b) and (m_m^c, χ^c) for (7-a), (7-b), and (7-c), respectively. After some simple algebra, they can be computed as follows

$$m_m^a = \frac{h_m^F}{\tau^F} - \frac{2 \exp\left(-\frac{\tilde{u}_{y_m}^2}{2}\right) - 2 \exp\left(-\frac{\tilde{l}_{y_m}^2}{2}\right)}{\sqrt{2\pi\tau^F} \left[\operatorname{erfc}\left(-\frac{\tilde{u}_{y_m}}{\sqrt{2}}\right) - \operatorname{erfc}\left(-\frac{\tilde{l}_{y_m}}{\sqrt{2}}\right) \right]}, \quad (13)$$

$$\chi^a = \frac{1}{\tau^F} - \frac{1}{M} \sum_{m=1}^M \left[\frac{2\tilde{u}_{y_m} \exp\left(-\frac{\tilde{u}_{y_m}^2}{2}\right) - 2\tilde{l}_{y_m} \exp\left(-\frac{\tilde{l}_{y_m}^2}{2}\right)}{\sqrt{2\pi\tau^F} \left[\operatorname{erfc}\left(-\frac{\tilde{u}_{y_m}}{\sqrt{2}}\right) - \operatorname{erfc}\left(-\frac{\tilde{l}_{y_m}}{\sqrt{2}}\right) \right]} + \left(m_m^a - \frac{h_m^F}{\tau^F} \right)^2 \right], \quad (14)$$

$$m_m^b = [(\tau^G \mathbf{I} + \mathbf{C}_t)^{-1} \mathbf{h}^G]_m, \quad (15)$$

$$\chi^b = \operatorname{Tr}[(\tau^G \mathbf{I} + \mathbf{C}_t)^{-1}] / M, \quad (16)$$

$$m_m^c = \frac{h_m^G + h_m^F}{\tau^G + \tau^F}, \quad (17)$$

$$\chi^c = \frac{1}{\tau^G + \tau^F}, \quad (18)$$

where $\operatorname{erfc}(z) = \frac{2}{\sqrt{\pi}} \int_z^\infty e^{-t^2} dt$ is the complementary error function (erfc) of the standard normal distribution, $\operatorname{Tr}[\cdot]$ is the trace of a matrix, and $[\cdot]_m$ is the m -th element of a vector.

In the special case of 1-bit quantization, i.e., sign measurements as described in (2), the results of (m_m^a, χ^a) in (13, 14) and g_m in (12) can be further simplified as follows

$$m_m^a = \frac{h_m^F}{\tau^F} + \frac{2y_m e^{-\frac{\tilde{l}^2}{2}}}{\sqrt{2\pi\tau^F} \operatorname{erfc}\left(\frac{y_m \tilde{l}}{\sqrt{2}}\right)}, \quad (19)$$

$$\chi^a = \frac{1}{\tau^F} - \frac{1}{M} \sum_{m=1}^M \left[\left(m_m^a - \frac{h_m^F}{\tau^F} \right)^2 - \frac{2y_m \tilde{l} e^{-\frac{\tilde{l}^2}{2}}}{\sqrt{2\pi\tau^F} \operatorname{erfc}\left(\frac{y_m \tilde{l}}{\sqrt{2}}\right)} \right], \quad (20)$$

$$g_m = \frac{y_m \sqrt{2\tau^F} e^{-\frac{\tilde{l}^2}{2}}}{\sqrt{\pi} \operatorname{erfc}\left(\frac{y_m \tilde{l}}{\sqrt{2}}\right)}, \quad (21)$$

where $\tilde{l} = -\sqrt{\tau^F} z_{t,m} - \frac{h_m^F}{\sqrt{\tau^F}}$.

Subsequently, by imposing the moment-matching conditions Minka (2001); Opper et al. (2005), i.e.,

$$m_m^a = m_m^b = m_m^c, \quad (22)$$

$$\chi^a = \chi^b = \chi^c, \quad (23)$$

one can obtain $(\mathbf{h}^F, \tau^F, \mathbf{h}^G, \tau^G)$ iteratively, and hence the targeted pseudo-likelihood score (11).

3.3 Resultant Algorithm: QCS-SGM+

By combining the pseudo-likelihood score (11) approximated via EP and the prior score from SGM, we readily obtain an enhanced version of QCS-SGM, dubbed as QCS-SGM+, using the annealed Langevin dynamics (ALD) (Song & Ermon, 2019). The details of QCS-SGM+ are shown

Algorithm 1: QCS-SGM+

Input: $\{\beta_t\}_{t=1}^T, \epsilon, \gamma, IterEP, K, \mathbf{y}, \mathbf{A}, \sigma^2$, quantization thresholds $\{[l_q, u_q] | q \in \mathcal{Q}\}$
Initialization: $\mathbf{x}_1^0 \sim \mathcal{U}(0, 1)$

```

1 for  $t = 1$  to  $T$  do
2    $\alpha_t \leftarrow \epsilon \beta_t^2 / \beta_T^2$ 
3   for  $k = 1$  to  $K$  do
4     Draw  $\mathbf{z}_t^k \sim \mathcal{N}(\mathbf{0}, \mathbf{I})$ 
5     Initialization:  $\mathbf{h}^F, \tau^F, \mathbf{h}^G, \tau^G$ 
6     for  $it = 1$  to  $IterEP$  do
7        $\mathbf{h}^G = \frac{\mathbf{m}^a}{\chi^a} - \mathbf{h}^F$ 
8        $\tau^G = \frac{1}{\chi^a} - \tau^F$ 
9        $\mathbf{h}^F = \frac{\mathbf{m}^b}{\chi^b} - \mathbf{h}^G$ 
10       $\tau^F = \frac{1}{\chi^b} - \tau^G$ 
11      Compute  $\nabla_{\mathbf{x}_t} \log p_{\beta_t}(\mathbf{y} | \mathbf{x}_t)$  as (11)
12       $\mathbf{x}_t^k = \mathbf{x}_t^{k-1} + \alpha_t \left[ \mathbf{s}\theta(\mathbf{x}_t^{k-1}, \beta_t) + \gamma \nabla_{\mathbf{x}_t} \log p_{\beta_t}(\mathbf{y} | \mathbf{x}_t) \right] + \sqrt{2\alpha_t} \mathbf{z}_t^k$ 
13    $\mathbf{x}_{t+1}^0 \leftarrow \mathbf{x}_t^K$ 
Output:  $\hat{\mathbf{x}} = \mathbf{x}_T^K$ 

```

in Algorithm 1 where the number of iterations of EP is denoted as $IterEP$. A scaling factor γ is introduced in QCS-SGM+, which is empirically found helpful to further improve the performance.

Note that while it seems from (15, 16) that matrix inversion $(\tau^G \mathbf{I} + \mathbf{C}_t)^{-1}$ is needed in each iteration for every \mathbf{C}_t , this is actually not the case since there exists one efficient implementation method using singular value decomposition (SVD) similar to Rangan et al. (2019); Meng & Kabashima (2022). Specifically, denote $\mathbf{A} = \mathbf{U}\Sigma\mathbf{V}^T$ as the SVD of \mathbf{A} and Σ^2 as the element-wise square of singular values, i.e., diagonal elements of Σ , then after some simple algebra, it can be shown that the terms \mathbf{m}^b, χ^b involving a matrix inverse can be efficiently computed as follows

$$\mathbf{m}^b = \mathbf{U} \text{diag} \left(\frac{\sigma^2 + \beta_t^2 \Sigma^2}{\tau_G(\sigma^2 + \beta_t^2 \Sigma^2) + 1} \right) \mathbf{U}^T \mathbf{h}^G, \quad (24)$$

$$\chi^b = \left\langle \frac{\sigma^2 + \beta_t^2 \Sigma^2}{\tau_G(\sigma^2 + \beta_t^2 \Sigma^2) + 1} \right\rangle, \quad (25)$$

where $\langle \cdot \rangle$ is the mean value of a vector. It can be seen from (24, 25) that one simply needs to replace the values of β_t, τ_G for different iterations. Hence, the main computational burden lies in the SVD of sensing matrix \mathbf{A} , but only one time is required in the whole QCS-SGM+.

4 Experiments

In this section, we empirically demonstrate the efficacy of the proposed QCS-SGM+ in various scenarios. In particular, following previous standard settings Rangan et al. (2019); Schniter et al. (2016); Tanaka (2018); Venkataraman et al. (2022); Zhu et al. (2022); Fan (2022), we investigate two popular kinds of general sensing matrices \mathbf{A} beyond row-orthogonal as follows:

(a) **ill-conditioned matrices** (Rangan et al., 2019; Schniter et al., 2016; Venkataraman et al., 2022; Fan, 2022): $\mathbf{A} = \mathbf{V}\Sigma\mathbf{U}^T$, where \mathbf{V} and \mathbf{U} are independent Harr-distributed matrices, and the nonzero singular values of \mathbf{A} satisfy $\frac{\lambda_i}{\lambda_{i+1}} = \kappa^{1/M}$, where κ is the condition number. Such matrices can have an arbitrary spectral distribution and often arise in practical applications (Venkataraman et al., 2022).

(b) **correlated matrices** Shiu et al. (2000); Zhu et al. (2022): \mathbf{A} is constructed as $\mathbf{A} = \mathbf{R}_L \mathbf{H} \mathbf{R}_R$, where $\mathbf{R}_L = \mathbf{R}_1^{\frac{1}{2}} \in \mathbb{R}^{M \times M}$ and $\mathbf{R}_R = \mathbf{R}_2^{\frac{1}{2}} \in \mathbb{R}^{N \times N}$, the (i, j) th element of both \mathbf{R}_1 and \mathbf{R}_2 is $\rho^{|i-j|}$ and ρ is termed as the correlation coefficient here, $\mathbf{H} \in \mathbb{R}^{M \times N}$ is a random matrix whose elements are drawn i.i.d. from $\mathcal{N}(0, 1)$.

Datasets: Same as Meng & Kabashima (2023), we consider three popular datasets: MNIST (LeCun & Cortes, 2010) , CIFAR-10 (Krizhevsky & Hinton, 2009), and CelebA (Liu et al., 2015). MNIST (LeCun & Cortes, 2010) are grayscale images of size 28×28 pixels so that the input dimension for MNIST is $N = 28 \times 28 = 784$ per image. CIFAR-10 (Krizhevsky & Hinton, 2009) consists of natural RGB images of size 32×32 pixels, resulting in $N = 32 \times 32 \times 3 = 3072$ inputs per image. For CelebA dataset (Liu et al., 2015), we cropped each face image to a 64×64 RGB image, resulting in $N = 64 \times 64 \times 3 = 12288$ inputs per image.

QCS-SGM+: For fair of comparison, same as QCS-SGM (Meng & Kabashima, 2023), the SGM model adopted here is the NCSNv2 (Song & Ermon, 2020) in all cases. Specifically, for MNIST, the NCSNv2 (Song & Ermon, 2020) was trained on the MNIST training dataset with a similar training set up as CIFAR-10 in Song & Ermon (2020), while for CIFAR-10, and CelebA, we use the pre-trained models available in this Link. For detailed hyper-paramters setting of QCS-SGM+, please refer to Appendix A.

Comparison Methods: We compare our QCS-SGM+ with not only the current state-of-the-art QCS-SGM (Meng & Kabashima, 2023), but also two other leading methods prior to QCS-SGM, namely BIPG (Liu et al., 2020) and OneShot (Liu & Liu, 2022). We use all the default settings as the associated open-sourced codes for QCS-SGM, BIPG, and OneShot.

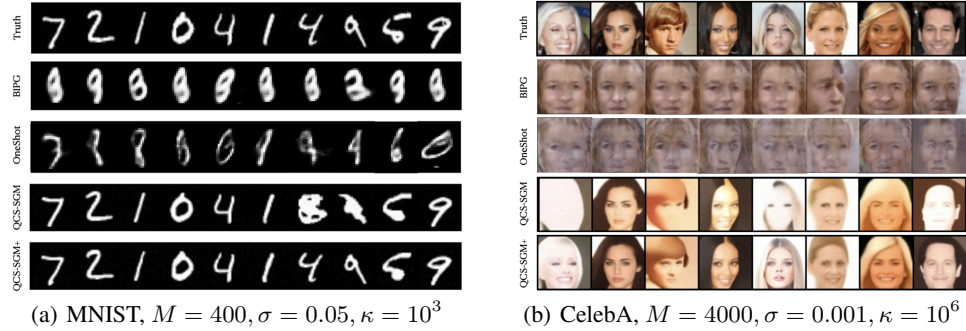


Figure 2: Qualitative comparisons between QCS-SGM+ and QCS-SGM, BIPG and OneShot under 1-bit CS on MNIST and CelebA for ill-conditioned \mathbf{A} ($\kappa = 10^3$ for MNIST and $\kappa = 10^6$ for CelebA) when $M \ll N$. It can be seen that QCS-SGM+ apparently outperforms the original QCS-SGM and other methods.

4.1 Qualitative Results

Figure 2 shows some qualitative results of QCS-SGM+ and QCS-SGM, BIPG, and OneShot under 1-bit CS for ill-conditioned \mathbf{A} . It can be seen from Figure 2 that the proposed QCS-SGM+ achieves remarkably better performances than all previous methods and can well reconstructs the target images from only a few $M \ll N$ sign measurements even when the sensing matrix \mathbf{A} is highly ill-conditioned. To further demonstrate the efficacy of QCS-SGM+ under different quantization resolutions (e.g., 1-3 bits), Figure 3 shows some results of QCS-SGM and QCS-SGM+, respectively, with condition number of \mathbf{A} being $\kappa = 10^3$ and $\sigma = 0.1$. It can be seen that QCS-SGM+ is able to generate clear images even with $M \ll N$ 1-3 bit noisy quantized measurements, whereas the original QCS-SGM yields only vague or blurry results. More results can be found in Appendix B.

4.2 Quantitative Results

In this section we provide some quantitative comparison between QCS-SGM+ and QCS-SGM in terms of the peak signal-to-noise ratio (PSNR). More results in terms of the structural similarity index measure (SSIM) (Wang et al., 2004) can be found in Appendix B. First, Figure 4 illustrates the PSNR results of QCS-SGM+ and QCS-SGM, in the case of 1-bit CS with MNIST, CIFAR-10, and CelebA, for ill-conditioned \mathbf{A} and correlated \mathbf{A} , respectively. It can be seen that in all cases, the proposed QCS-SGM+ achieves much better performances, demonstrating the superiority of QCS-SGM+ over QCS-SGM for more general sensing matrices \mathbf{A} .

Furthermore, we evaluate the effect of additive Gaussian noise $\mathbf{n} \sim \mathcal{N}(\mathbf{n}; 0, \sigma^2 \mathbf{I})$ by conducting experiments on 1-bit CS with different levels of noise standard deviation (std) σ . As shown in Figure



Figure 3: Reconstructed images on CIFAR-10 with QCS-SGM and QCS-SGM+, respectively, under 1-3 bit CS when the condition number of \mathbf{A} is 1000, $M = 2000$, $\sigma = 0.1$. QCS-SGM+ achieves significantly better results than QCS-SGM.

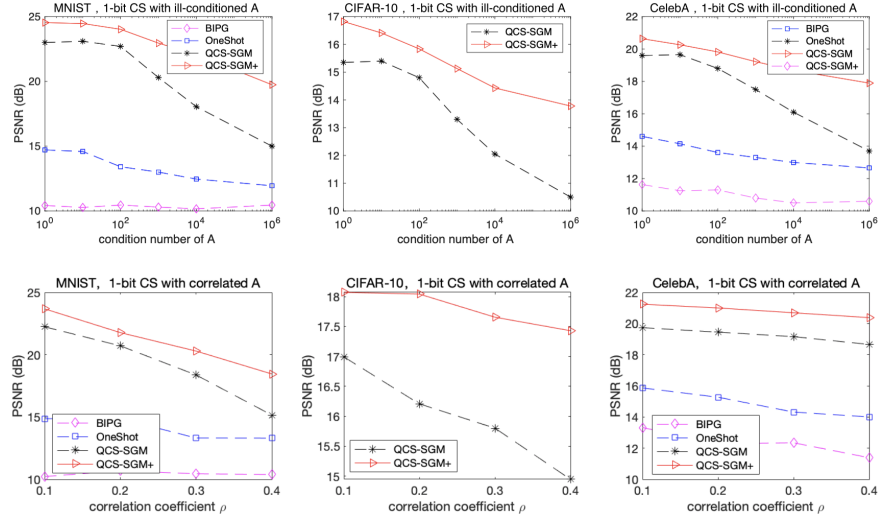


Figure 4: Quantitative comparisons between QCS-SGM+ and existing methods under 1-bit CS for MNIST, CIFAR-10, and CelebA when the sensing matrices \mathbf{A} are ill-conditioned and correlated, respectively. The number of noisy measurements are set to be $M = 400, 2000, 4000$ for MNIST, CIFAR-10, and CelebA, respectively, all satisfying $M \ll N$. In all cases, QCS-SGM+ apparently outperforms QCS-SGM, OneShot, and BIPG.

5, due to the potential dithering effect, QCS-SGM+ with noise can sometimes achieve slightly better results than that without noise. Generally, QCS-SGM+ is robust to noise and can achieve good results in a large range of \mathbf{n} , while significantly outperforming QCS-SGM.

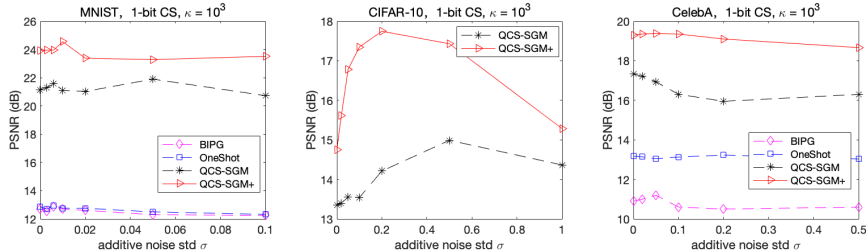


Figure 5: Quantitative comparisons between QCS-SGM+ and existing methods under 1-bit CS with different levels of additive Gaussian noise for ill-conditioned \mathbf{A} with condition number $\kappa = 10^3$. The number of measurements are set to be $M = 400, 2000, 4000$ for MNIST, CIFAR-10, and CelebA, respectively, all satisfying $M \ll N$. In all cases, QCS-SGM+ apparently outperforms QCS-SGM, OneShot, and BIPG.

5 Conclusion

In this paper, we propose an improved version of QCS-SGM called QCS-SGM+ for general sensing matrices. By viewing the likelihood computation as a Bayesian inference problem, QCS-SGM+ efficiently approximates the intractable likelihood score using the well-known EP. To verify the effectiveness of QCS-SGM, we conducted experiments on a variety of baseline datasets, demonstrating that QCS-SGM+ significantly outperforms QCS-SGM by a large margin. There are several limitations of QCS-SGM+. For example, QCS-SGM+ requires EP message passing, which is computationally slower than QCS-SGM. Also, same as QCS-SGM, it requires a large number of iterations to generate one posterior sample. As future work, it is important to further reduce the complexity of QCS-SGM+ and develop more efficient alternatives with more advanced diffusion models. Moreover, a theoretical analysis of both QCS-SGM and QCS-SGM+ is also an important future direction.

References

Asim, M., Daniels, M., Leong, O., Ahmed, A., and Hand, P. Invertible generative models for inverse problems: mitigating representation error and dataset bias. In *International Conference on Machine Learning*, pp. 399–409. PMLR, 2020.

Awasthi, P., Balcan, M.-F., Haghtalab, N., and Zhang, H. Learning and 1-bit compressed sensing under asymmetric noise. In *Conference on Learning Theory*, pp. 152–192. PMLR, 2016.

Bora, A., Jalal, A., Price, E., and Dimakis, A. G. Compressed sensing using generative models. In *International Conference on Machine Learning*, pp. 537–546. PMLR, 2017.

Boufounos, P. T. and Baraniuk, R. G. 1-bit compressive sensing. In *2008 42nd Annual Conference on Information Sciences and Systems*, pp. 16–21, 2008. doi: 10.1109/CISS.2008.4558487.

Candès, E. J. and Wakin, M. B. An introduction to compressive sampling. *IEEE signal processing magazine*, 25(2):21–30, 2008.

Dai, W. and Milenkovic, O. Information theoretical and algorithmic approaches to quantized compressive sensing. *IEEE transactions on communications*, 59(7):1857–1866, 2011.

Donoho, D. L. Compressed sensing. *IEEE Transactions on information theory*, 52(4):1289–1306, 2006.

Fan, Z. Approximate message passing algorithms for rotationally invariant matrices. *The Annals of Statistics*, 50(1):197–224, 2022.

Goodfellow, I., Pouget-Abadie, J., Mirza, M., Xu, B., Warde-Farley, D., Ozair, S., Courville, A., and Bengio, Y. Generative adversarial nets. In Ghahramani, Z., Welling, M., Cortes, C., Lawrence, N., and Weinberger, K. (eds.), *Advances in Neural Information Processing Systems*, volume 27. Curran Associates, Inc., 2014. URL <https://proceedings.neurips.cc/paper/2014/file/5ca3e9b122f61f8f06494c97b1afccf3-Paper.pdf>.

Hand, P. and Joshi, B. Global guarantees for blind demodulation with generative priors. *Advances in Neural Information Processing Systems*, 32, 2019.

Ho, J., Jain, A., and Abbeel, P. Denoising diffusion probabilistic models. *Advances in Neural Information Processing Systems*, 33:6840–6851, 2020.

Ihara, M., Iwata, K., Suematsu, N., and Mimura, K. Typical performance of sparse signal recovery from a linear measurement with large coherence. In *2018 International Symposium on Information Theory and Its Applications (ISITA)*, pp. 427–431. IEEE, 2018.

Jacques, L., Laska, J. N., Boufounos, P. T., and Baraniuk, R. G. Robust 1-bit compressive sensing via binary stable embeddings of sparse vectors. *IEEE transactions on information theory*, 59(4):2082–2102, 2013.

Jalal, A., Arvinte, M., Daras, G., Price, E., Dimakis, A. G., and Tamir, J. Robust compressed sensing mri with deep generative priors. *Advances in Neural Information Processing Systems*, 34:14938–14954, 2021.

Jung, H. C., Maly, J., Palzer, L., and Stollenwerk, A. Quantized compressed sensing by rectified linear units. *IEEE transactions on information theory*, 67(6):4125–4149, 2021.

Kingma, D. P. and Welling, M. Auto-encoding variational bayes. *arXiv preprint arXiv:1312.6114*, 2013.

Krizhevsky, A. and Hinton, G. Learning multiple layers of features from tiny images. Technical report, Citeseer, 2009.

LeCun, Y. and Cortes, C. MNIST handwritten digit database. 2010. URL <http://yann.lecun.com/exdb/mnist/>.

Liu, J. and Liu, Z. Non-iterative recovery from nonlinear observations using generative models. In *Proceedings of the IEEE/CVF Conference on Computer Vision and Pattern Recognition*, pp. 233–243, 2022.

Liu, Z., Luo, P., Wang, X., and Tang, X. Deep learning face attributes in the wild. In *Proceedings of International Conference on Computer Vision (ICCV)*, December 2015.

Liu, Z., Gomes, S., Tiwari, A., and Scarlett, J. Sample complexity bounds for 1-bit compressive sensing and binary stable embeddings with generative priors. In *International Conference on Machine Learning*, pp. 6216–6225. PMLR, 2020.

Manoel, A., Krzakala, F., Tramel, E., and Zdeborova, L. Swept approximate message passing for sparse estimation. In *International Conference on Machine Learning*, pp. 1123–1132. PMLR, 2015.

Meng, X. and Kabashima, Y. Diffusion model based posterior sampling for noisy linear inverse problems. *arXiv preprint arXiv:2211.12343*, 2022.

Meng, X. and Kabashima, Y. Quantized compressed sensing with score-based generative models. In *International Conference on Learning Representations*, 2023.

Meng, X., Wu, S., and Zhu, J. A unified bayesian inference framework for generalized linear models. *IEEE Signal Processing Letters*, 25(3):398–402, 2018.

Minka, T. P. Expectation propagation for approximate bayesian inference. In *Proceedings of the Seventeenth conference on Uncertainty in artificial intelligence*, pp. 362–369, 2001.

Nichol, A. Q. and Dhariwal, P. Improved denoising diffusion probabilistic models. In *International Conference on Machine Learning*, pp. 8162–8171. PMLR, 2021.

Opper, M., Winther, O., and Jordan, M. J. Expectation consistent approximate inference. *Journal of Machine Learning Research*, 6(12), 2005.

Pan, X., Zhan, X., Dai, B., Lin, D., Loy, C. C., and Luo, P. Exploiting deep generative prior for versatile image restoration and manipulation. *IEEE Transactions on Pattern Analysis and Machine Intelligence*, 2021.

Plan, Y. and Vershynin, R. Robust 1-bit compressed sensing and sparse logistic regression: A convex programming approach. *IEEE Transactions on Information Theory*, 59(1):482–494, 2012.

Plan, Y. and Vershynin, R. One-bit compressed sensing by linear programming. *Communications on Pure and Applied Mathematics*, 66(8):1275–1297, 2013.

Radford, A., Metz, L., and Chintala, S. Unsupervised representation learning with deep convolutional generative adversarial networks. *arXiv preprint arXiv:1511.06434*, 2015.

Rangan, S., Schniter, P., and Fletcher, A. K. Vector approximate message passing. *IEEE Transactions on Information Theory*, 65(10):6664–6684, 2019.

Rezende, D. and Mohamed, S. Variational inference with normalizing flows. In *International conference on machine learning*, pp. 1530–1538. PMLR, 2015.

Schniter, P., Rangan, S., and Fletcher, A. K. Vector approximate message passing for the generalized linear model. In *2016 50th Asilomar conference on signals, systems and computers*, pp. 1525–1529. IEEE, 2016.

Shiu, D.-S., Foschini, G. J., Gans, M. J., and Kahn, J. M. Fading correlation and its effect on the capacity of multielement antenna systems. *IEEE Transactions on communications*, 48(3):502–513, 2000.

Sohl-Dickstein, J., Weiss, E., Maheswaranathan, N., and Ganguli, S. Deep unsupervised learning using nonequilibrium thermodynamics. In *International Conference on Machine Learning*, pp. 2256–2265. PMLR, 2015.

Song, Y. and Ermon, S. Generative modeling by estimating gradients of the data distribution. *Advances in Neural Information Processing Systems*, 32, 2019.

Song, Y. and Ermon, S. Improved techniques for training score-based generative models. *Advances in neural information processing systems*, 33:12438–12448, 2020.

Song, Y., Sohl-Dickstein, J., Kingma, D. P., Kumar, A., Ermon, S., and Poole, B. Score-based generative modeling through stochastic differential equations. In *International Conference on Learning Representations*, 2020.

Tanaka, T. Performance analysis of l_1 -norm minimization for compressed sensing with non-zero-mean matrix elements. In *2018 IEEE International Symposium on Information Theory (ISIT)*, pp. 401–405. IEEE, 2018.

Venkataraman, R., Kögler, K., and Mondelli, M. Estimation in rotationally invariant generalized linear models via approximate message passing. In *International Conference on Machine Learning*, pp. 22120–22144. PMLR, 2022.

Wainwright, M. J. and Jordan, M. I. *Graphical models, exponential families, and variational inference*. Now Publishers Inc, 2008.

Wang, Z., Bovik, A. C., Sheikh, H. R., and Simoncelli, E. P. Image quality assessment: from error visibility to structural similarity. *IEEE transactions on image processing*, 13(4):600–612, 2004.

Xu, Y. and Kabashima, Y. Statistical mechanics approach to 1-bit compressed sensing. *Journal of Statistical Mechanics: Theory and Experiment*, 2013(02):P02041, feb 2013. doi: 10.1088/1742-5468/2013/02/p02041. URL <https://doi.org/10.1088/1742-5468/2013/02/p02041>.

Xu, Y., Kabashima, Y., and Zdeborová, L. Bayesian signal reconstruction for 1-bit compressed sensing. *Journal of Statistical Mechanics: Theory and Experiment*, 2014(11):P11015, nov 2014. doi: 10.1088/1742-5468/2014/11/p11015. URL <https://doi.org/10.1088/1742-5468/2014/11/p11015>.

Zhu, J., Meng, X., Lei, X., and Guo, Q. A unitary transform based generalized approximate message passing. *arXiv preprint arXiv:2210.08861*, 2022.

Zymnis, A., Boyd, S., and Candes, E. Compressed sensing with quantized measurements. *IEEE Signal Processing Letters*, 17(2):149–152, 2009.

A Hyper-parameter Setting of QCS-SGM+

As shown in Algorithm 1, there are several hyper-parameters in the proposed QCS-SGM+, including $\{\beta_t\}_{t=1}^T, \epsilon, \gamma, IterEP, K$. Among them, the values of $\{\beta_t\}_{t=1}^T$ and K are exactly the same as the pre-trained SGM model, i.e., once the pre-trained SGM model is given, $\{\beta_t\}_{t=1}^T$ and K are fixed as the same value as the SGM. The step size ϵ is set to be the same as QCS-SGM, which is a constant value (here, same as QCS-SGM, we set ϵ to be $\epsilon = 0.002$ in all the experiments), though some further improvement can be expected with a careful fine-tuning of it.

Regarding the scaling factor γ of QCS-SGM+, it is set as follows

$$\gamma = \xi \frac{\|s_{\theta}(\mathbf{x}_t^{k-1}, \beta_t)\|}{\|\nabla_{\mathbf{x}_t} \log p_{\beta_t}(\mathbf{y} \mid \mathbf{x}_t)\|}, \quad (26)$$

where $\xi > 0$ is another induced scalar hyper-parameter. In the original QCS-SGM, no γ is introduced, i.e., it is simply set to be a fixed value $\gamma = 1$. However, it is empirically found that adding a proper scaling factor γ leads to a better performance (as shown in Figure 6). The choice of the form in (26) is inspired from Jalal et al. (2021).

Regarding the number of iterations $IterEP$ of QCS-SGM+, it is empirically found that 3-5 iterations are enough in most cases (as shown in Figure 6). As a result, if there is no further illustration, the experimental results shown in this paper are all using $IterEP = 5$ by default.

To illustrate the effect of γ and $IterEP$ of QCS-SGM+, Figure 6 shows 1-bit CS results of QCS-SGM+ on various datasets with (w.t.) and without (w.o.) scaling factor γ for different number of EP iterations $IterEP$. Specifically, we set $\xi = 0.5$ for both MNIST and CIFAR-10, and $\xi = 0.3$ for CelebA for QCS-SGM+ w.t. γ in all the related experiments. It can be seen that in both cases with and without γ , QCS-SGM+ converges with 3-5 EP iterations. Interestingly, when the sensing matrix \mathbf{A} deviates from row-orthogonal matrix, i.e., the condition number becomes much larger than 1, QCS-SGM+ w.o. γ apparently outperforms the original QCS-SGM, demonstrating the efficacy of EP in QCS-SGM+. Furthermore, QCS-SGM+ w.t. γ further improves QCS-SGM+ w.o. γ by introducing the scaling factor γ . Overall, the proposed QCS-SGM+ significantly outperforms the original QCS-SGM.

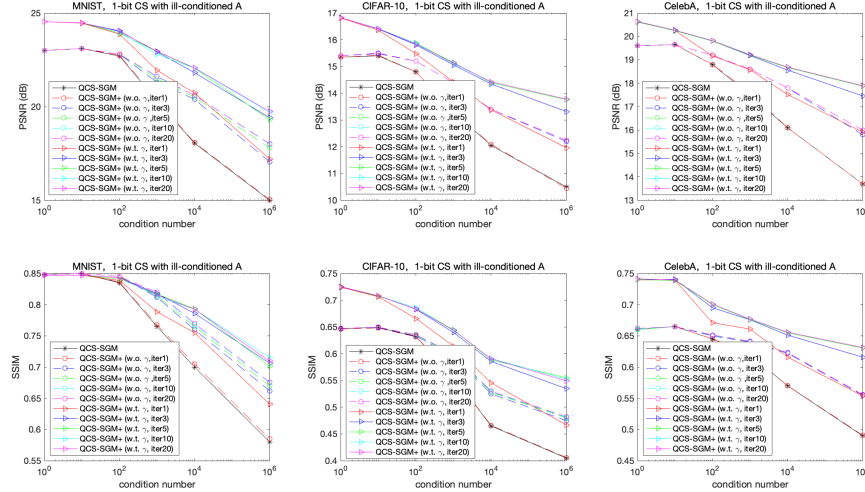


Figure 6: 1-bit CS results of QCS-SGM+ on various datasets with (w.t.) and without (w.o.) scaling factor γ for different number of EP iterations $IterEP$. In this example, the sensing matrix \mathbf{A} used is ill-conditioned with different condition numbers. Note that both PSNR and SSIM results are shown.

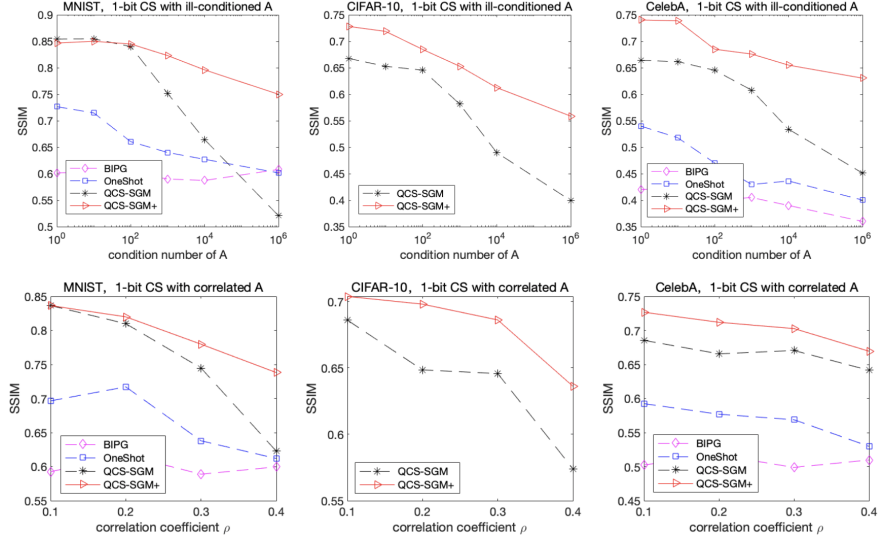


Figure 7: Quantitative comparisons (in terms of SSIM) of the proposed QCS-SGM+ and the original QCS-SGM under 1-bit CS for MNIST, CIFAR-10, and CelebA datasets when the measurement matrices \mathbf{A} are ill-conditioned and correlated, respectively. The number of measurements are set to be $M = 400, 2000, 4000$ for MNIST, CIFAR-10, and CelebA, respectively, all satisfying $M \ll N$. In all cases, QCS-SGM+ apparently outperforms QCS-SGM.

B Additional Results

All the experiments are conducted on one NVIDIA Tesla V100. In this appendix, we show some additional results apart from those in the main text.

B.1 Quantitative Results in terms of SSIM

In this section, we provide additional quantitative results in terms of the structural similarity index measure (SSIM). As shown in Figure 7 and Figure 8, similar to the PSNR metric, the proposed QCS-SGM+ significantly outperforms QCS-SGM as well as BIPG and OneShot in terms of SSIM. Note that results of BIPG and OneShot for CIFAR-10 are not shown since there is a lack of pre-trained model in their open-sourced code.

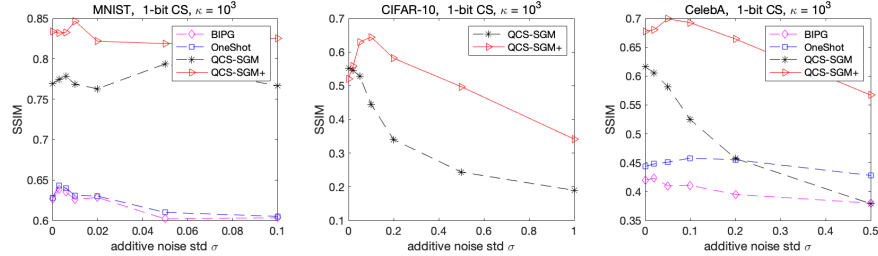


Figure 8: Quantitative comparisons (in terms of SSIM) of the proposed QCS-SGM+ and the original QCS-SGM under 1-bit CS with different levels of additive Gaussian noise for ill-conditioned \mathbf{A} with condition number $\kappa = 10^3$. The number of measurements are set to be $M = 400, 2000, 4000$ for MNIST, CIFAR-10, and CelebA, respectively, all satisfying $M \ll N$. In all cases, QCS-SGM+ apparently outperforms QCS-SGM.

B.2 Additional Qualitative Results

In this section, we provide additional qualitative results in various settings, as shown in Figures 9 - 17. The results in Figures 9 - 17 empirically demonstrate that our proposed QCS-SGM+ remarkably outperforms the original QCS-SGM for general matrices beyond mere row-orthogonality.

| Truth | QCS-SGM+ (ours) | QCS-SGM |
|-----------------|-----------------|-----------------|
| 7 2 1 0 4 1 4 9 | 7 2 1 0 4 1 4 9 | 7 2 1 0 4 1 4 9 |
| 5 9 0 6 9 0 1 5 | 5 9 0 6 9 0 1 5 | 5 9 0 6 9 0 1 5 |
| 9 7 8 4 9 6 6 5 | 9 7 3 4 9 6 6 5 | 9 7 8 4 9 6 6 5 |
| 4 0 7 4 0 1 3 1 | 4 0 7 4 0 1 3 1 | 4 0 7 4 0 1 3 1 |
| 3 4 7 2 7 1 2 1 | 3 4 7 2 7 1 2 1 | 3 4 7 2 8 1 2 1 |
| 1 7 4 2 3 5 1 2 | 1 7 4 2 3 5 1 2 | 1 7 4 2 3 5 1 2 |
| 4 4 6 3 5 5 6 0 | 4 4 6 3 5 5 6 0 | 4 4 6 3 5 5 6 0 |
| 4 1 9 5 7 8 9 3 | 4 1 9 5 7 8 9 3 | 4 1 9 5 7 8 8 3 |

(a) 1-bit CS with ill-conditioned $\mathbf{A}, \kappa = 10^3, M = 400, \sigma = 0.1$

| Truth | QCS-SGM+ (ours) | QCS-SGM |
|-----------------|-----------------|-----------------|
| 7 2 1 0 4 1 4 9 | 7 2 1 0 4 1 4 9 | 7 2 1 0 4 1 8 8 |
| 5 9 0 6 9 0 1 5 | 5 9 0 6 9 0 1 5 | 5 9 0 6 9 0 1 5 |
| 9 7 8 4 9 6 6 5 | 9 7 3 4 9 6 6 5 | 9 7 8 4 9 6 6 5 |
| 4 0 7 4 0 1 3 1 | 4 0 7 4 0 1 3 1 | 4 0 7 4 0 1 3 1 |
| 3 4 7 2 7 1 2 1 | 3 4 7 2 7 1 2 1 | 3 4 7 2 7 1 2 1 |
| 1 7 4 2 3 5 1 2 | 1 7 4 2 3 5 1 2 | 1 7 9 2 3 5 1 2 |
| 4 4 6 3 5 5 6 0 | 4 4 6 3 5 5 6 0 | 4 4 6 3 6 5 6 8 |
| 4 1 9 5 7 8 9 3 | 4 1 9 5 7 8 9 3 | 4 1 9 5 7 8 9 3 |

(b) 1-bit CS with correlated $\mathbf{A}, \rho = 0.4, M = 400, \sigma = 0.1$

Figure 9: Comparison of QCS-SGM and QCS-SGM+ (ours) for 1-bit CS on MNIST with (a) ill-conditioned \mathbf{A} and (b) correlated \mathbf{A} , respectively. It can be seen that in both cases QCS-SGM+ outperforms QCS-SGM remarkably.

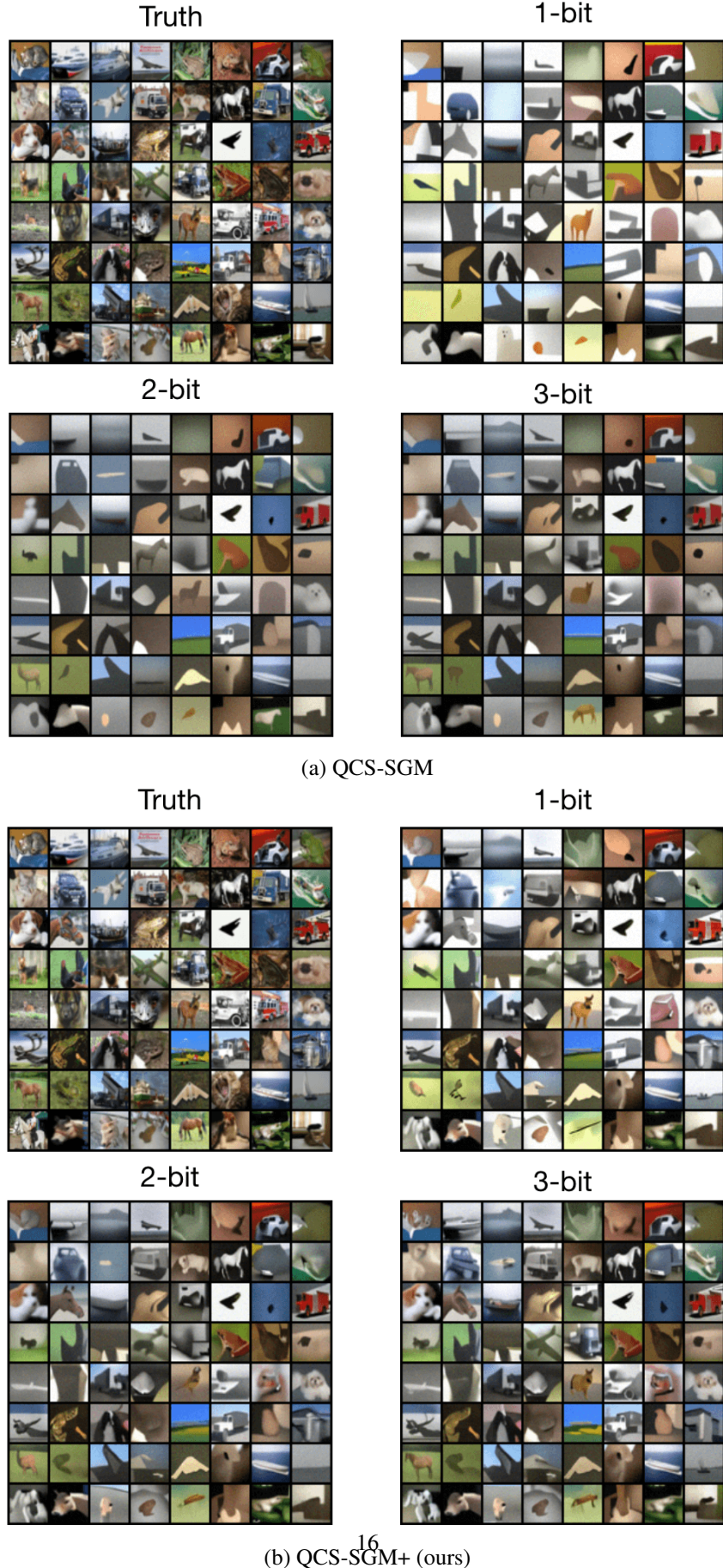
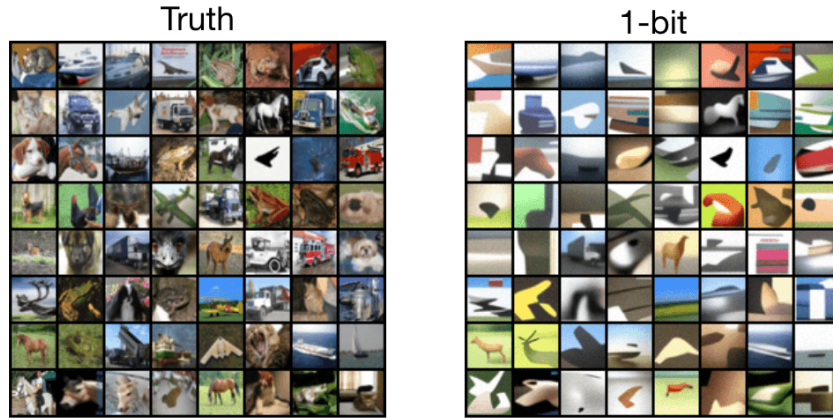
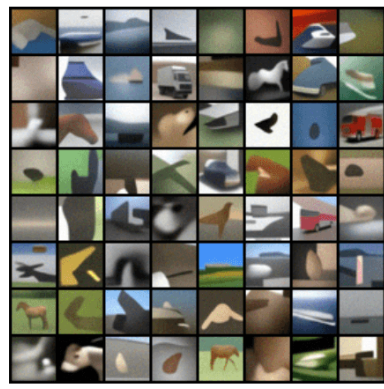


Figure 10: Results of QCS-SGM+ and QCS-SGM under 1-3 bit CS on CIFAR-10 for ill-conditioned \mathbf{A} ($\kappa = 10^3$) when $M = 2000$, $\sigma = 0.1$. QCS-SGM+ outperforms QCS-SGM remarkably.



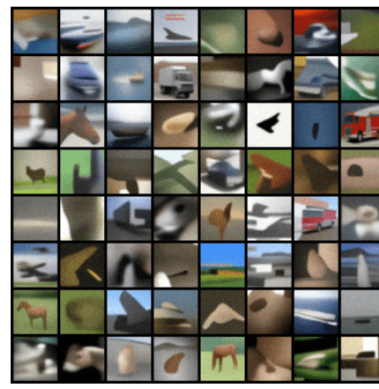
2-bit



1-bit



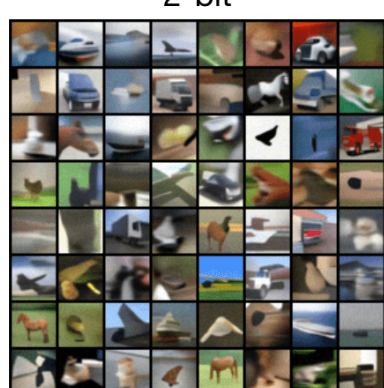
3-bit



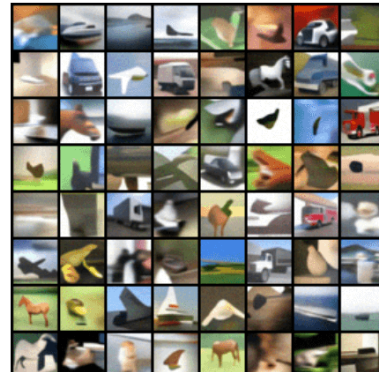
(a) QCS-SGM



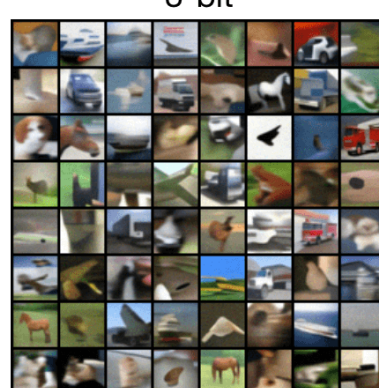
2-bit



1-bit



3-bit



(b) QCS-SGM+ (ours)

Figure 11: Results of QCS-SGM+ and QCS-SGM under 1-3 bit CS on CIFAR-10 for correlated \mathbf{A} ($\rho = 0.4$) when $M = 2000, \sigma = 0.1$. QCS-SGM+ outperforms QCS-SGM remarkably.



Figure 12: Results of QCS-SGM under 1-3 bit CS on CelebA for ill-conditioned \mathbf{A} ($\kappa = 10^3$) when $M = 4000, \sigma = 0.1$.



Figure 13: Results of QCS-SGM+ (ours) under 1-3 bit CS on CelebA for ill-conditioned \mathbf{A} ($\kappa = 10^3$) when $M = 4000$, $\sigma = 0.1$. It can be seen that QCS-SGM+ outperforms QCS-SGM in Figure 12 remarkably.



Figure 14: Results of QCS-SGM under 1-3 bit CS on CelebA for ill-conditioned \mathbf{A} ($\kappa = 10^6$) when $M = 4000, \sigma = 0.1$.



Figure 15: Results of QCS-SGM+ (ours) under 1-3 bit CS on CelebA for ill-conditioned \mathbf{A} ($\kappa = 10^3$) when $M = 4000$, $\sigma = 0.1$. It can be seen that QCS-SGM+ outperforms QCS-SGM in Figure 14 remarkably.



Figure 16: Results of QCS-SGM under 1-3 bit CS on CelebA for correlated \mathbf{A} ($\rho = 0.4$) when $M = 4000, \sigma = 0.1$.



Figure 17: Results of QCS-SGM+ (ours) under 1-3 bit CS on CelebA for correlated \mathbf{A} ($\rho = 0.4$) when $M = 4000, \sigma = 0.1$. It can be seen that QCS-SGM+ outperforms QCS-SGM in Figure 16 remarkably.